Arabian Journal of Chemistry (2022) **15**, 103464

King Saud University

Arabian Journal of Chemistry

www.ksu.edu.sa
www.sciencedirect.com

ORIGINAL ARTICLE

Improvement of anti-inflammatory and anticancer activities of poly(lactic-co-glycolic acid)-sulfasalazine microparticle via density functional theory, molecular docking and ADMET analysis

Alireza Soltani [a,b], Afrasyab Khan [c], Hassan Mirzaei [d], Marjan Onaq [b], Masoud Javan [e], Samaneh Tavassoli [b], Nosrat O Mahmoodi [a], Ali Arian Nia [f], Asieh Yahyazadeh [a,*], Aref Salehi [d,*], Seyed Reza Khandoozi [f,*], Razieh Khaneh Masjedi [g], Md Lutfor Rahman [h,*], Mohd Sani Sarjadi [h], Shaheen M. Sarkar [i], Chia-Hung Su [j,*]

[a] *Department of Chemistry, Faculty of Science, University of Guilan, P.O. Box 41335-1914 Rasht, Iran*
[b] *Golestan Rheumatology Research Center, Golestan University of Medical Science, Gorgan, Iran*
[c] *Reserch Institute of Mechanical Engineering, Department of Vibration Testing and Equipment Condition Monitoring, South Ural State University, Lenin Prospect 76, Chelyabinsk 454080, Russian Federation*
[d] *Ischemic Disorders Research Center, Golestan University of Medical Sciences, Gorgan, Iran*
[e] *Department of Physics, Faculty of Sciencesy of Medical Science, Gorgan, Iran*
[f] *Cancer Research Center, Golestan University of Medical Sciences, Gorgan, Iran*
[g] *Department of Chemical Sciences, Bernal Institute, University of Limerick, Limerick, Ireland*
[h] *Faculty of Science and Natural Resources, Universiti Malaysia Sabah, 88400 Kota Kinabalu, Sabah, Malaysia*
[i] *Department of Applied Science, Technological University of the Shannon, Moylish Park, Limerick V94 EC5T, Ireland*
[j] *Department of Chemical Engineering, Ming Chi University of Technology, New Taipei City, Taiwan*

Received 8 July 2021; accepted 27 September 2021
Available online 5 October 2021

KEYWORDS

Sulfasalazin;

Abstract In the present study, we assessed improvement of anti-inflammatory activity and drug delivery of sulfasalazine (SSZ) by the poly(lactic-co-glycolic acid), (PLGA), in H_2O and dichloromethane (DCM) environments via density functional theory (DFT), ADMET, and molecular

* Corresponding authors.
E-mail addresses: yahyazadehphd@yahoo.com (A. Yahyazadeh), yahyazadehphd@yahoo.com (A. Yahyazadeh), yahyazadehphd@yahoo.com (A. Yahyazadeh), yahyazadehphd@yahoo.com (A. Yahyazadeh), yahyazadehphd@yahoo.com (A. Yahyazadeh), salehia@goums.ac.ir (A. Salehi), Drkhandoozi92002@yahoo.com (S. Reza Khandoozi), lotfor@ums.edu.my (M. Lutfor Rahman), chsu@mail.mcut.edu.tw (C.-H. Su).
Peer review under responsibility of King Saud University.

Production and hosting by Elsevier

https://doi.org/10.1016/j.arabjc.2021.103464

PLGA;
Gibbs free solvation energy;
Anti-inflammatory activity;
Solubility

docking. Our calculated results based on binding energy and thermodynamic parameter represents that the interaction between SSZ and PLGA in Complex **A** via double hydrogen bonds is stronger in comparison with Complex B. The analysis of Ultraviolet–visible (UV–VIS) spectra proved the interaction of SSZ with PLGA by time-dependent density functional theory (TDDFT). Infrared (IR) spectra demonstrated that the structure of PLGA was shifted in the presence of the SSZ. The interaction of SSZ with PLGA leads to an increase in dipole moment and higher solubility with more negative Gibbs free solvation energy (ΔG_{solv}) values and lowering of the energy gap (E_g). The obtained results by Molecular docking demonstrates that the interaction of SSZ via its carboxylate group with PLGA (complex **A**) had a strong interaction towards the binding pocket of the target and as a potential inhibitor of the COX-2, TNF-α, and IL-1 receptors at the binding site as compared with the complex **B**.

1. Introduction

Because of their tailorable features, poly-lactic-co-glycolic acid (PLGA) microparticles are rapidly gaining significance in the field of nanomedicine (Rezvantalab et al., 2020). PLGA polymers are the Food and Drug Administration (FDA) approved that consists of a synthetic copolymer of α-hydroxy propanoic acid (lactic acid) and hydroxy acetic acid (glycolic acid) (Li and Jiang, 2018; Rezvantalab et al., 2018; Rezvantalab and Moraveji, 2019). PLGA microparticles because of its biodegradable and biocompatible nature are particularly attractive as one of the most commonly applied to deliver DNA vaccines and noncondensing microparticles in intestinal gene delivery (Bolhassani et al., 2014; Amirmahani et al., 2017; Ghavidast et al., 2014; Rineh et al., 2007; Ghavidast and N.O. , 2016). In this research, we used PLGA microparticles to delivery of SSZ in both polar (H_2O) and nonpolar (CH_2Cl_2) solvents and its effects on inhibition of COX-2 activity and and proinflammatory cytokines like TNF-α and IL-1.

SSZ is known as a disease-modifying anti-rheumatic drug (DMARD) and nonsteroidal anti-inflammatory (NSAID) generally employed for the decrement of rheumatoid arthritis, Crohn's disease, ulcerative colitis, inflammatory bowel disease, and immunosuppressive attributes (Malaekehpoor et al., 2020; Savalia and Chatterjee, 2018). Different studies have been done to investigate non-steroidal anti-inflammatory drugs (NSAIDs) containing celecoxib and diclofenac sodium incorporated PLGA nanoparticles (NPs) to reduce the toxicity and side effects of some drugs (Harirforoosh et al., 2016; Tuncay and S.C¸ alis¸ H.S. Kas¸ M.T. Ercan, I. Peksoy, A. A. Hincal, , 2000). Stipa *et al.* have shown prediction of the interactions of PLA and PLGA nanocarriers with Paracetamol, Prednisolone, and Isoniazid by molecular dynamics simulations (Stipa et al., 2021). Ansari *et al.* demonstrated the binding energy of gemcitabine in PLGA is greater in comparison to camptothecin by a molecular dynamics simulation that this result can leads to a decrease in the delivery rate from the system (Ansari et al., 2018). Aghaei et al. have shown nonionic surfactant vesicles as novel delivery systems for SSZ, in which the amount of drug released was 22.4 wt% after one day (Aghaei et al., 2021a). Kokcu *et al.* demonstrated the nontoxic effect of tripeptide Gly-His-Lys (GHK) loaded PLGA NPs on L929 cells and they found a spherical morphology of GHK loaded PLGA can lead to alterations in the wavenumbers happening at the characteristic peaks of GHK in histidine, peptide and carboxyl groups (Kokcu et al., 2020). Abdolahi *et al.* theoretically found the negative adsorption energy in the interaction between the gold decorated $B_{12}N_{12}$ nanocluster and the SSZ and the calculated results demonstrated that the donor state red shift of the fermi states located on Au-orbitals is because of substantial alterations in coulomb quantum well (QW) depth between those (Abdolahi et al., 2020). Budama-Kilinc demonstrated the encapsulation of piperine within PLGA by using spectroscopic, imaging, and molecular docking simulation methods. It have shown that piperine could be used for inflammation and pain treatment due to significant inhibition of COX-1 and COX-2 cytokines (Budama-Kilinc, 2019). In addition, in silico investigations was done in water and DCM environments via density functional theory (DFT), ADMET, and molecular docking calculations for SSZ as an oral drug candidate with anti-inflammatory and analgesic features.

2. Computational method

The minimum potential energy surface of the anti-inflammatory drug and their complexes with PLGA carriers were calculated via density functional dispersion correction (DFT-D) at the level of B3LYP-D combined with the basic set 6–31 + G(d,p) from Gaussian 09 software (Becke, 1988; Lee et al., 1988). This level of theory has presented to be accurate sufficient for a vast diversity of non-covalently interacting dimer systems between the drugs and the different polymer- carriers (Moniruzzaman et al., 2018; Rahman et al., 2016). After the geometry optimizations, binding energies were computed by zero-point corrected energies (ZPE) at the B3LYP-D/6–31 + G(d,p) level of theory with the help of the following generic formula:

$$E_{bin} = (E_{SSZ/PLGA} + ZPE) - - E_{PLGA}(E_{SSZ} + 0PE) \quad (1)$$

where E_{PLGA} is the total energy of pure PLGA microparticle, E_{SSZ} is the total energy of free SSZ molecule and $E_{SSZ/PLGA}$ is the total energy of the formed complex. The polarizable continuum model (PCM) was chosen to assess the impact of the solvent on the adsorption mechanism of the SSZ onto PLGA in H_2O and DCM environments. Physicochemical features of the interaction systems were also calculated based on the definition of quantum molecular descriptors (QMD):

$$\mu = -\frac{1}{2}(I + A) \quad (2)$$

$$\chi = -\mu \tag{3}$$

$$\eta = \frac{1}{2}(I - A) \tag{4}$$

$$S = \frac{1}{2\eta} \tag{5}$$

$$\omega = \frac{\mu^2}{2\eta} \tag{6}$$

where A is electron affinity, I is ionization potential, S is global softness, μ is chemical potential, χ is electronegativity, η is global hardness, and ω is electrophilicity index (Parr et al., 1978; Parr et al., 1999). According to, Koopmans' theorem, the order of I and A can be determined as the negative orbital energies of the HOMO (highest occupied molecular orbital), $-E_{HOMO}$ and the LUMO (lowest unoccupied molecular orbital), $-E_{LUMO}$ (Koopmans, 1933). Molecular docking studies were carried out using Auto Dock software (4.2) (Morris et al., 2009). The Crystal Structure of TNF-alpha (PDB ID: 2AZ5), structure of IL1A-S100A13 complex (PDB ID: 2L5X) and cyclooxygenase-2 (prostaglandin synthase-2) (PDB ID: 1CX2) were retrieved from Protein Data Bank. The structure of the proteins prepared following as cognate ligand was removed, hydrogen atoms were added and nonpolar hydrogen were merged, Kollman charge was allocated using Auto Dock Tools (ADT). The Lamarckian genetic algorithm was used for the local search method. A grid map of 60x60x60 with 0.375 Å grid spacing was designated for the preparation of autogrid (Aghaei et al., 2021b; Cao et al., 2021). 100 GA runs was used for docking. To evaluate the amino acid residues evolves in the binding pocket of protein with compounds, we applied Maestro 11.0 Schrodinger program for the creation of 2D and 3D presentation.

3. Results and discussion

3.1. Binding energy and thermodynamic analysis

At first, we focused our efforts to estimate the binding energy of SSZ adsorbed on the PLGA microparticle in two orientations. Fig. 1 represents the SSZ via its carboxylate group interacts with the PLGA (complex **A**) via double hydrogen bonds with a E_{bin} of −0.62 eV (minimum energy) in a water environment and −0.65 eV in DCM environment (maximum energy). A dimer model formed in complex **A** for both environments by intermolecular hydrogen bonds. Recently, Cao *et al.* have found that the interaction between the sulfasalazine and naproxen via double hydrogen bonds with a binding energy of −0.64 eV (Cao et al., 2021). We also computed the zero-point corrected energy (ZPE) for the SSZ drug interacts with the PLGA microparticle in DCM environment. The ZPE values in complexes **A** and **B** are about −0.66 and −0.39 eV, respectively. The evaluation of binding energy by ZPE demonstrates that the interaction of SSZ with PLGA in complex **B** is physisorption in nature which is in accordance with the calculated results from thermodynamic parameters. The values of the thermodynamic parameters for complexes **A** and **B** in DCM environment were calculated. The calculated values of Gibbs free solvation energy (ΔG_{solv}) and enthalpy (ΔH_{solv}) for complex **A** in order is found to be −0.15 and −0.65 eV and these values in complex **B** in order is + 0.14 and −0.38 eV. The amount of ΔG_{solv} difference with the enthalpy is because of the entropic effect (Cao et al., 2021). The negative values of ΔH_{solv} in complex **A** represent the exothermic process, the negative value of ΔG_{solv} demonstrates the spontaneous interaction between the SSZ and the PLGA in the thermodynamic approach. In confirmation of our results, the electron localization function (ELF) map in Fig. 1 represents when SSZ becomes close to PLGA microparticle in complex **A** via double hydrogen bonds and the more stable the microparticle becomes compared with the complex **B** (Rezvantalab et al., 2020).

The values of dipole moment (DM) for the pure PLGA and SSZ molecules are found to be 4.50 and 7.82 Debye, respectively. After the interaction of SSZ with PLGA, the DM values in complex **A** and **B** are found to be 11.80 and 10.82 Debye, respectively. The notable increment in DM values demonstrates an intensifying of the interactions SSZ and PLGA with nonpolar solvents like DCM, and will thus improve their solubility in physiological media via increase the internal molecular electric field (Md. Abdur Rauf et al., 2015). In fact, the molecular field created by electric dipoles moments causes polarization in adjacent molecular structures and increases their reactivity due to electrostatic force. Mulliken population analysis (MPA) demonstrates that complex **A** had a strong charge-transfer of about 0.563 |e| from SSZ to PLGA in comparison with complex **B** (0.214 |e|).

The QMD value η in the SSZ and PLGA systems were 1.79 and 3.73 eV, which significantly changed in complex A and B with values of 1.80 and 1.81 eV, respectively. The complex **B** and **A** display different chemical stability to those of the pure PLGA, with η and μ values of −3.73 and −4.40 eV, respectively. This means that the interaction of molecules induces significant alterations in the carrier electronic features and leads to enhance chemical reactivity (Pasban and Raissi, 2021). Complex **B** has a lower electrophilicity index (6.39 eV) in comparison with complex **A** (6.51 eV) that is similar with the value of electrophilicity index of the pure PLGA (6.51 eV). Hence, the ω demonstrates the ability of the fragments to accept electrons. With interaction between the SSZ and PLGA, the values of ω in complex **B** decreased during the interaction of the SSZ drug with PLGA which confirmed that this complex with more tendency to donor electron compared to the corresponding pure systems (Table 1).

Fig. 2 represents the infrared (IR) curves of SSZ interact with PLGA in complex **A** and **B**. The IR curve of the pure PLGA demonstrates the bands of the OH at 3739 and 3829 cm^{-1} and the carbonyl bands appeared at 1803 and 1817 cm^{-1}. Kokcu *et al.* experimentally demostrated the C═O stretching vibration of the PLGA polymer, this vibration was marked at 1759 cm^{-1} (Kokcu et al., 2020). The FT-IR spectrum of SSZ had a band at 1676 cm^{-1} that corresponded to the C═O stretching vibration (Cao et al., 2021). In complex **A**, the carbonyl bands for both SSZ and PLGA molecules appeared at 1680 and 1752 cm^{-1}, while the hydroxyl group of the pure SSZ and PLGA appeared at 3457 and 3831 cm^{-1}, respectively. The C—H aromatic ring in complex **A** appeared at 3182–3242 cm^{-1}, while in the pure SSZ appeared at 3182–3241 cm^{-1}. In complex **B**, two carbonyl bands for PLGA molecule appeared at 1770 and 1797 cm^{-1} and in the SSZ molecule appeared at 1723 cm^{-1}, while the hydroxyl group of SSZ and PLGA appeared at 3409 and

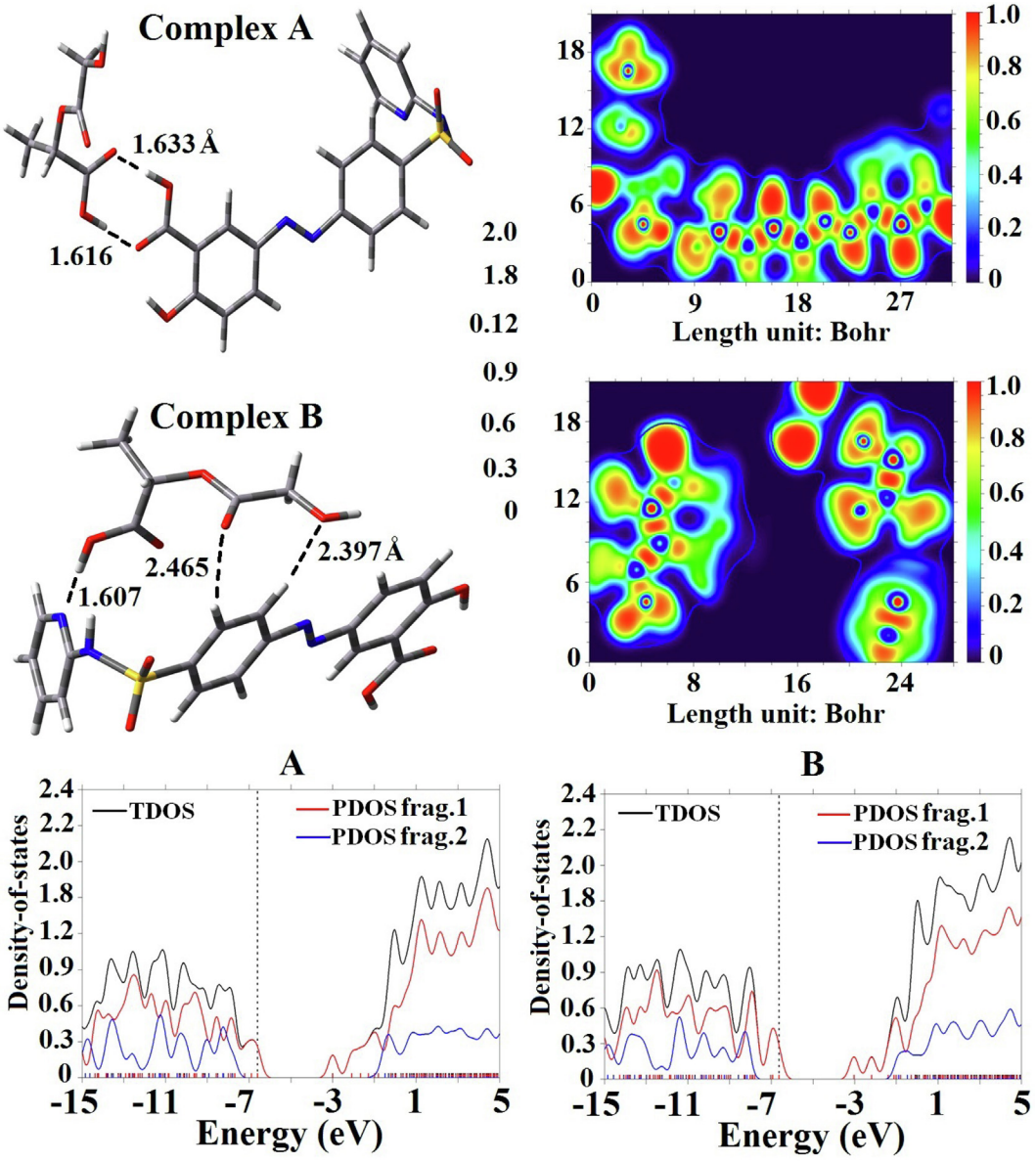

Fig. 1 Optimized geometries and ELF maps of SSZ interact with PLGA in different configurations.

Table 1 Calculated binding energy (E_{ads}), chemisorption bond distance (D), dipole moment (μ_D), HOMO energy (E_{HOMO}), LUMO energy (E_{LUMO}), energy gap (E_g), Fermi level energy (E_F) and quantum molecular descriptors for SSZ, PLGA, complex **B,** and complex **A** in DCM environment.

Property	$E_{HOMO}(eV)$	$E_{LUMO}(eV)$	$E_g(eV)$	$\Delta E_g(\%)$	$E_F(eV)$	$I(eV)$	$A(eV)$	$\chi(eV)$	$\mu(eV)$	$\eta(eV)$	$S(eV^{-1})$	$\omega(eV)$
SSZ	−6.62	−3.04	3.58	–	−4.83	6.62	3.04	4.83	−4.83	1.79	0.28	6.51
PLGA	−8.12	−0.67	7.45	–	−4.40	8.12	0.67	4.40	−4.40	3.73	0.13	2.59
A	−6.64	−3.04	3.60	51.68	−4.84	6.64	3.04	4.84	−4.84	1.80	0.28	6.51
B	−6.62	−3.00	3.62	51.41	−4.81	6.62	3.0	4.81	−4.81	1.81	0.28	6.39

3746 cm^{-1}, respectively. The C-H aromatic ring in complex **B** appeared at 3199–3252 cm^{-1}.

Fig. 3 presents the highest occupied molecular orbital (HOMO) and lowest unoccupied molecular orbital (LUMO) wavefunctions for SSZ interact with PLGA microparticles. For complex **A**, HOMO are more localized on the C—C and N═N bonds of the drug (λ_{max} = 372 nm) with the main contribution from HOMO to LUMO (88%) and the LUMO is more localized in both aromatic rings of the drug. On the other hand, the minor contribution from HOMO-7 to LUMO + 1 (32%) happens where these are mostly localized on the C—C bonds and O atoms of salicylic acid of the drug. In contrast, HOMO and LUMO of the complex **B** are mostly localized on the C-C and N = N bonds of drug (λ_{max} = 365 nm) with

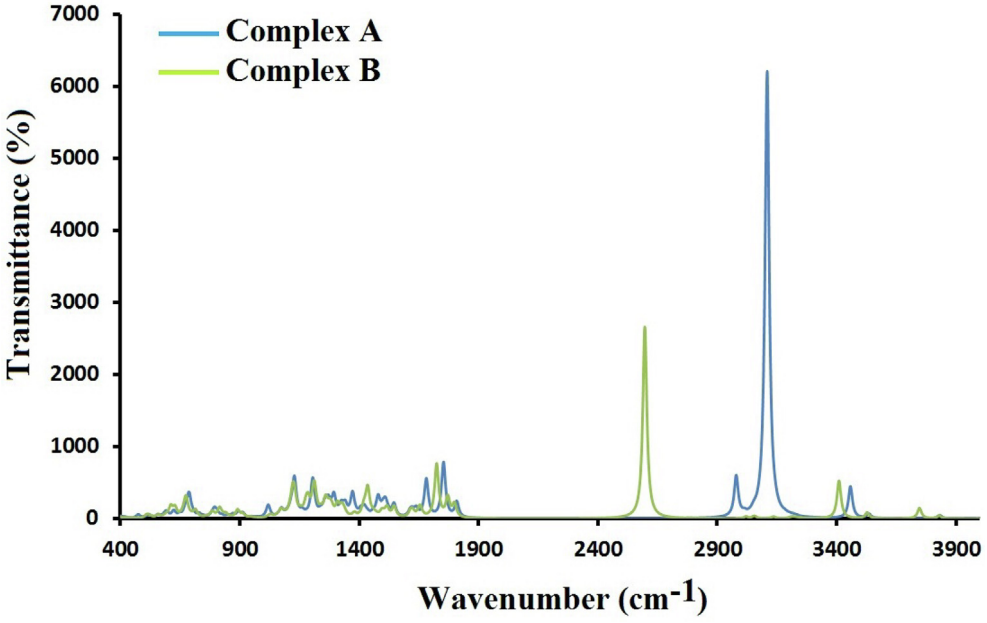

Fig. 2 IR spectrum of SSZ interacts with PLGA.

the main contribution from HOMO to LUMO (97%), while HOMO-3 is more localized on the C, O, N, H, and S atoms throughout a drug and LUMO + 3 of the complex B are mostly localized on the aromatic and pyridine rings of drug.

The interaction of SSZ with the PLGA microparticle was also calculated through spectroscopic techniques. According to Fig. 4, in complex **A**, maximum absorption band appeared at 372 nm and oscillator strength of 0.74 and the minimum band at 233 nm and oscillator strength of 0.20 because of intraligand $\pi \rightarrow \pi^*$ and $n \rightarrow \pi^*$ transitions. In contrast with complex **A**, in complex **B**, the maximum absorption band appeared at 365 nm and oscillator strength of 0.93 and minimum the band at 216 nm and oscillator strength of 0.14. Aghaei et al. have shown the absorption band for SSZ loaded to ST8 micellar/niosomal vesicles at 234 and 357 nm (Mirzaei et al., 2017). According to the obtained results, we see a blue shift in complex B compared to complex A, so that the absorption threshold has shifted to the blue region of about 17 nm. Regarding the fact that the single-particle energy gap in complexes A is 0.27 lower than B, the optical gap in structure A is 0.42 smaller than the optical gap in complex B, which indicates to bounded the excitonic energy levels. According to the relation of:

$$E_{exciton} = Eg_{single-particle} - Eg_{optical}$$

We have the excitons in complex A and B with the energy of -1.72 , -2.12 eV, respectively. These results show that the electron-hole coupling in complex B is stronger than complex A.

The AOCs calculated for the four compounds: Complex B, SSZ, PLGA and Complex A are approximately comparable, ranging from 2.62 to 2.67, with a slight variance between them. On the other hand, this number is calculated for SSZ is equivalent to 2.63. Since concentration units of AOC is reported for SSZ, its conversion to concentration for other three is accessible.

3.2. Anti-inflammatory and Anti-cancer activities

In this study, we used the binding affinity for the selected systems toward three targets TNF-alpha (PDB ID: 2AZ5), IL1A (PDB ID: 2L5X) and cyclooxygenase-2 (COX-2) (PDB ID: 1CX2) by the AutoDock (4.2) software. Finding amino acid residues involved in the receptor selected complexes (SSZ, PLGA, complex **A**, and complex **B**) was determined in active site of targets. The obtained results exhibited that system consist of complex **A** is the most potent inhibitor of COX-2 (PDB ID: 1CX2) compared to complex **B**. As shown in Table 2, the values of binding energy (BE) for complex **A** in the binding pocket of targets in the order of 2AZ5, 2L5X, and 1CX2 was found to be -9.8, -9.4, and -11.6 (kcal/mol). On the other hand, interaction of complex **A** with cyclooxygenase-2 (COX-2) target in comparison to two targets TNF-alpha and IL1A had the highest binding affinity. Complex **A** from its carboxylate group binds in the binding pocket of the 1CX2 target adjacent to Ala2, Ile87, Leu6, Pro5 and Ala3 by the hydrophobic interactions (Mirzaei et al., 2017) and also binds with other amino acid residues like Phe64, Leu80, Ala151, Leu152, and Pro153. Moreover, the complex **A** binds with amino acid residues like Glu46, Asp125, Glu465, Arg150, Arg465, Arg469, Arg44, Lys468, Lys83, Thr129, Thr130, Gln42, Lys41, Asn43, Ser471, Tyr122, Gly63, Thr62, and Thr76 via polar interactions. Furthermore, complex A is established in the active site of the receptor (1CX2) using five hydrogen bonds with the amino acid residues of the receptor such as Arg44, Glu465, Ala151 and Thr130. Hydrogen bond lengths were 2.07, 2.14, 3.01, 3.02, and 2.64 Å respectively. 3D structure of the binding site revealed that complex **A** was located in the pockets of the receptor(1CX2) (Fig. 5). Regarding molecular docking results illustrated that complex **A** had lower binding affinity to the COX2 receptor whereas the complex revealed a strong interaction with amino acids chains of the target in the active site and lead to inhibition more effectively

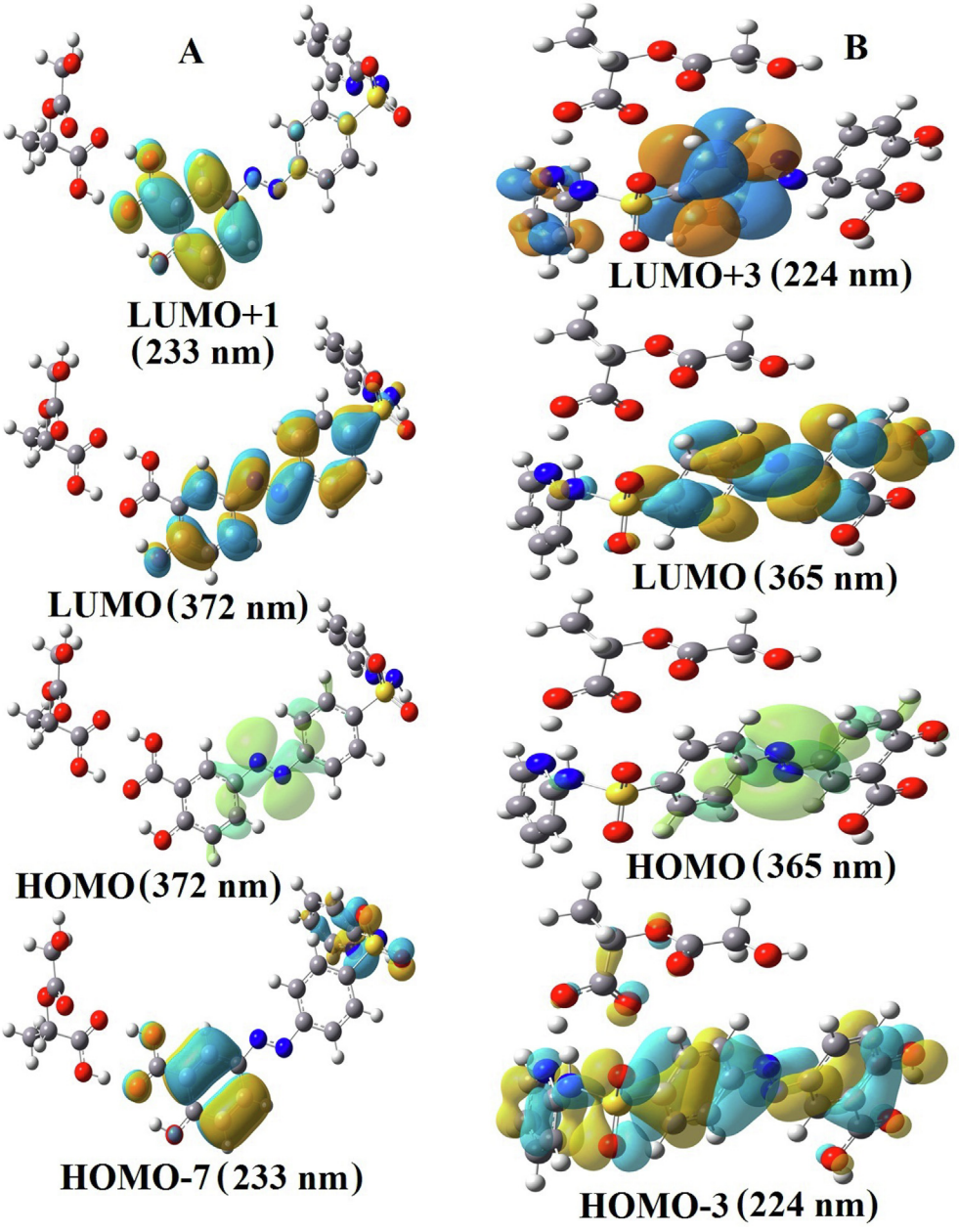

Fig. 3 HOMO and LUMO transitions for the SSZ-PLGA complex.

the binding pocket of the receptor comparison with the other complexes.

Human Epidermal Growth Factor Receptor type 2 (HER2) results in inhibition of over-expression in breast cancer. Targets (PDB ID: 3RCD and 5O4G) applied to determine the binding affinity of the selected complexes toward HER2 receptor. The obtained results exhibited that complex **A** inhibited HER2 receptor compared to complex **B**. As shown in Table 1, the values of the binding energy (BE) for complex **A** in the binding pocket of targets in the order of 3RCD and 5O4G was found to be −8.9 and −8.6 (kcal/mol). Complex **A** binds in the binding pocket of the 3RCD target adjacent to Ala879, Phe864, Ala751, Leu852, Leu726, Val734, and Leu755 by the hydrophobic interactions (Ermondi et al., 2004; Xu et al., 2018). Moreover, complex **A** binds with amino acid residues like Arg849, Gly729, His878, Lys753, Ser728, Asp880, Thr862, Asp863, Gly727, THr798, Thr798, Thr875, Glu874, Gly865, Asp873, and Ser763 via polar interactions. Furthermore, complex **A** is stabilized in the active site of the HER2 target by four hydrogen bonds with the amono acid residues such as Thr862, Asp863, and Thr875 (Daze et al.,). Hydrogen bond lengths were 2.84, 3.10, 3.01, 1.46, and 2.53 Å respectively (Fig. 5).

To compare of molecular docking results revealed that interaction of complex **A** with COX2 target in comparison to other targets like TNF-alpha, IL1A, and HER2 receptors had the lowest binding affinity. On the other hand, complex **A** had established in the binding site of COX-2 and result in inhibition more effectively the active site of the receptor compared to the other receptors. In addition, comparison of the

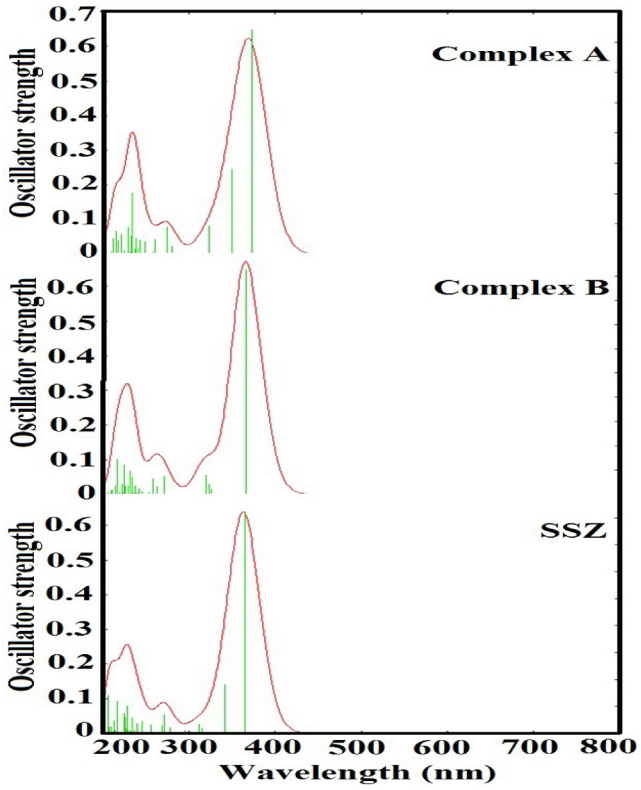

Fig. 4 UV–Visible spectra of SSZ encapsulated within PLGA.

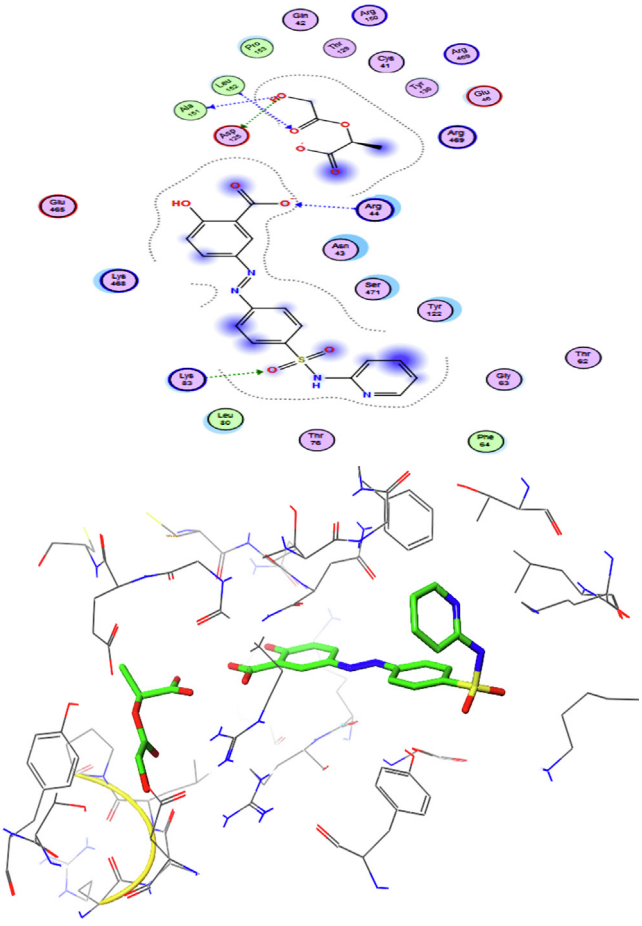

Fig. 5 Presentation of 2D and 3D models of interactions between complex **A** and COX-2 (PDB ID: 1CX2).

chemical structure of complexes exhibited that carboxylate moiety of SSZ in complex **A** connected with the carboxylate group of PLGA. Whereas SSZ and PLGA in complex **B** connected differently. The results demonstrated how the two interconnected molecules are extremely important in the binding affinity and occupy active sites of targets. In general, polar and nonpolar interactions may play an essential role in occupying the binding site. Likewise, molecular orientation can be effective in binding affinity. Accordingly, complex **A** could be a potent inhibitor of the COX-2, TNF-α, IL-1, and HER2 receptors at the active site.

3.3. Drug likeness and ADMET prediction

In order to elucidate ADMET (absorption, distribution, metabolism, excretion, and toxicity) and drug likness properties selected compounds analyzed for acceptance of . the Lipinski's Rule of 5. Complex A and B showed good drug likness characteristics therefore; were selected for further consideration (Table 3). The pharmacological properties of compounds were considered according to Lipinski's law. As seen in Table 3 absorption and permeability for compounds in the body occurs when the molecular weight is less than 500 Dalton, LogP less than 5, Hydrogen bond acceptors and donors are less than 10 and 5 respectively. In addition, logS also expresses solubility. As illustrated in Table 4, almost all compounds was compiled Lipinski's ''Rule of 5''. The log P values for the complex A and B were 2.7 (unit), (Table 3) while the calculated log

Table 2 Molecular docking simulations results for the complexes and TNF-α receptor (PDB ID: 2AZ5), IL-1 receptor (PDB ID: 2L5X) and COX-2 receptor (PDB ID:1CX2).

Compound	PDB ID: 2AZ5		PDB ID:2L5X		PDB ID:1CX2	
	BE (kcal/mol)	Ki (μM)	BE (kcal/mol)	Ki (μM)	BE (kcal/mol)	Ki (μM)
Complex B	−8.8	9.4	−8.5	10.4	−10.8	4.3
SSZ	−7.9	10.2	−7.6	11.8	−10.2	5.6
PLGA	−7.1	11.6	−6.8	12.5	−7.6	9.9
Complex A	−9.8	8.7	−9.4	9.7	−11.6	3.4

Table 3 Drug-likeness properties of compounds.

Compound	Log S	MW	Clog P	HBA	HBD	NRB	MR	TPSA	DL
ref	> -4	–	< = 5	< = 10	< = 5	< = 10	40–130	< 140	–
Complex B	−3.4	546	2.7	11	5	9	131	165	0.52
SSZ	−5.1	398	3.7	7	3	6	100	141	0.7
PLGA	−0.02	148	−1	4	2	3	31	84	0.94
Complex A	−3.4	546	2.7	11	5	9	131	164	0.52

Abbreviations:LogS: Logarithm of water solubility; MW: molecular weight; logP: Logarithm of compound partition coefficient between *n*-octanol and water; HBA: Number of hydrogen bonds acceptors; HBD: Number of hydrogen bond donors; TPSA: Topological polar surface area; NRB:Number of rotatable bonds, MR: Molecular refractivity, DL: Drug likeness.

Table 4 ADMET profile of compounds.

Compound	BBB	HIA	Caco2	P-GI	CYP450-2C9	CYP450-2D6	CYP450-3A4	AMES	CIG	HPT	AOC
ref	–	–		No	No	No	No	No	No	No	–
Complex B	Yes	Yes	No	No	Yes	No	No	No	No	toxic	2.67
SSZ	Yes	Yes	No	No	Yes	No	No	No	No	No	2.63
PLGA	Yes	Yes	No	No	No	No	No	No	No	No	2.66
Complex A	Yes	Yes	No	No	No	No	No	No	No	No	2.62

Abbreviations: BBB: Blood-Brain Barrier; HIA: Human Intestinal Absorption, P-GI: P-glycoprotein inhibitor, CIG: Carcinogens, HPT: hepatotoxicity, AOC: Acute oral Toxicity.

S values of −3.4 (unit) were identified for the complexes. moreover, the log P and log S values for PLGA was predicted to be −1 and −0.02 (unit), respectively. The Topological polar surface area (TPSA) values of PLGA rised from 84 to 165 (Complex B) and 164 (SSZ) in addition to the interaction of the PLGA surface the nanocages. TPSA is an important factor that plays an essential role in the permeability of bioactive compounds. Compounds with a PSA less than 140 Å have proper permeability. Hereby, rising TPSA value lead to decline permeability of the membrane and low TPSA associated with high absorption (Srivastava et al., 2020). Estimation of oral bioavailability are carried out to the whole selected compounds, possessing rotating bonds below 10, result in decreasing Configuration flexibility. Furthermore, compound PLGA have molar refractivity less than 130 and the other compounds have higher values. Topological polar surface area (TPSA) related to passive molecule transport through membranes. Complex A, B, and SSZ have TPSA values higher than 140 Å, and PLGA has an equal of 31 Å. Moreover, obtained results revealed that all compounds have a calculated logs value moderately. In addition, evaluation of ADMET properties exhibited that selected compounds have low oral bioavailability and High intestinal absorption (Table 4) and also All selected compounds had no Caco-2 penetrability, wheras all compounds are non-inhibitors of membrane p-glycoproteins and all of them be able to penetrate BBB. Additionally, almost all compounds were predicted to be non-inhibitor of CYP (CYP3A4, CYP2D6, and CYP2C9) and also no-carcinogenicity, no-mutagenicity (AMES) and hepatotoxicity.

4. Conclusions

We demonstrated improvement of anti-inflammatory activity and drug delivery of SSZ by the PLGA in H_2O and DCM environments via DFT, ADMET, and molecular docking. Our calculated results based on binding energy and thermodynamic parameter represents that the interaction between SSZ and PLGA in Complex **A** via double hydrogen bonds is stronger in comparison with Complex B. The study of molecular docking exhibits complex A containing SSZ and PLGA has a strong binding affinity with TNF-a , IL-1 and COX-2 receptors in comparison with the other complexes and besides the complex A inhibited effectively TNF-α and IL-1 receptors. Furthermore, physicochemical properties such as absorption, distribution, metabolism, excretion, and toxicity (ADMET), as well as drug-likeness, demonstrated that complex A had intersting ADMET properties compare to the other complexes and had a potential inhibition of inflammation.

Declaration of Competing Interest

The authors declare that they have no known competing financial interests or personal relationships that could have appeared to influence the work reported in this paper.

Acknowledgements

We gratefully acknowledge financial support from Golestan University of Medical Science (Research Project Grant No. 990308036).

The authors are thankful to the Russian Government and research institute of Mechanical Engineering, Department of Vibration Testing and Equipment Condition Monitoring, South Ural State University, Lenin prospect 76, Chelyabinsk, 454080, Russian Federation for their support to this work.

References

Rezvantalab, S., Keshavarz Moraveji, M., Khedri, M., Maleki, R., 2020. An insight into the role of riboflavin ligand in the self-

assembly of poly(lactic-co-glycolic acid)-based nanoparticles – a molecular simulation and experimental approach. Soft Matter 16 (22), 5250–5260.
Li, X., Jiang, X., 2018. Adv. Drug Deliv. Rev. 128, 101–114.
Rezvantalab, S., Drude, N.I., Moraveji, M.K., Güvener, N., Koons, E. K., Shi, Y., Lammers, T., Kiessling, F., 2018. Front. Pharmacol. 9.
Rezvantalab, S., Moraveji, M.K., 2019. RSC Adv. 9, 2055–2072.
Bolhassani, A., Javanzad, S., Saleh, T., Hashemi, M., Aghasadeghi, M.R., Sadat, S.M., 2014. Polymeric nanoparticles Potent vectors for vaccine delivery targeting cancer and infectious diseases. Hum. Vaccin. Immunother. 10 (2), 321–332.
Amirmahani, N., Mahmoodi, N.O., Mohammadi Galangash, M., Ghavidast, A., 2017. Mohammadi Galangash, Advances in nanomicelles for sustained drug delivery. J. Ind. Eng. Chem. 55, 21–34.
Ghavidast, A., Mahmoodi, N.O., Zanjanchi, M.A., 2014. Synthesis and photochromic properties of disulfide-1, 3-diazabicyclo [3.1. 0] hex-3-ene functionalized silver nanoparticles. J. Mol. Liq. 198, 128–133.
A. Rineh, N. Mahmoodi, M. Abdollahi, A. Foroumadi, M. Sorkhi, A. Shafiee, Synthesis, Analgesic and Anti-Inflammatory Activity of 4-(2-Phenoxyphenyl)semicarbazones 340 (2007) 409-415.
Ghavidast, A., Mahmoodi, N.O., 2016. A comparative study of the photochromic compounds incorporated on the surface of nanoparticles. J. Mol. Liq. 216, 552–564.
Malaekehpoor, Seyedeh Mina, Derakhshandeh, Katayon, Haddadi, Rasool, Nourian, Alireza, Ghorbani-Vaghei, Ramin, 2020. A polymer coated MNP scaffold for targeted drug delivery and improvement of rheumatoid arthritis. Polym. Chem. 11 (13), 2408–2417.
Savalia, R., Chatterjee, S., 2018. Sensing of sulfasalazine–cysteine transporter inhibitor with platinum nanoflowers decorated on carbon nanotubes by electrochemical reduction. Sensors Actuat. B Chem. 277, 39–46.
Harirforoosh, S., West, K.O., Murrell, D.E., Denham, J.W., Panus, P. C., Hanley, G.A., 2016. Assessment of celecoxib poly(lactic-co-glycolic) acid nanoformulation on drug pharmacodynamics and pharmacokinetics in rats. Eur. Rev. Med. Pharmacol. Sci. 20, 4818–4829.
Tuncay, M., Alis, S.C., Kas, H.S., Ercan, M.T., Peksoy, I., Hincal, A. A., 2000. Diclofenac sodium incorporated PLGA (50:50) microspheres: formulation considerations and in vitro/in vivo evaluation. Int. J. Pharm. 195, 179–188.
Stipa, P., Marano, S., Galeazzi, R., Minnelli, C., Mobbili, G., Laudadio, E., 2021. Prediction of drug-carrier interactions of PLA and PLGA drug-loaded nanoparticles by molecular dynamics simulations. Eur. Polym. J. 147, 110292.
Ansari, Mohabbat, Moradi, Sajad, Shahlaei, Mohsen, 2018. A molecular dynamics simulation study on the mechanism of loading of gemcitabine and camptothecin in poly lactic-co-glycolic acid as a nano drug delivery system. J. Mol. Liq. 269, 110–118.
Aghaei, M., Erfani-Moghadam, V., Soltani, A., Abdolahi, N., Cordani, M., Moazen Rad, S., Balakheyli, H., 2021a. Non-Ionic Surfactant Micelles/Vesicles as Novel Systems to enhance solubility of Sulfasalazine: Evaluation of the Physicochemical and Cytotoxic Properties. J. Mol. Struct. 1230, 129874.
Kokcu, Y., Kecel-Gunduz, S., Budama-Kilinc, Y., Cakir-Koc, R., Bicak, B., Zorlu, T., Ozel, A.E., Akyuz, S., 2020. Structural analysis, molecular dynamics and docking calculations of skin protective tripeptide and design, characterization, cytotoxicity studies of its PLGA nanoparticles. J. Mol. Struct. 1200, 127046.
Abdolahi, N., Singla, P., Soltani, A., Javan, M., Aghaei, M., Heidari, F., Sedighi, S., 2020. Gold decorated $B_{12}N_{12}$ nanocluster as an effective sulfasalazine drug carrier: A theoretical investigation. Physica E 124, 114296.
Budama-Kilinc, Y., 2019. Piperine Nanoparticles for Topical Application: Preparation Characterization, In vitro and In silico Evaluation. ChemistrySelect 4, 11693–11700.
A.D. Becke Density-functional exchange-energy approximation with correct asymptotic behavior. Phys Rev A 38(1988) 3098-3100.
Lee, C., Yang, W., Parr, R.G., 1988. Development of the Colle-Salvetti correlation-energy formula into a functional of the electron density. Phys. Rev. B 37, 785–789.
Moniruzzaman, M.J., Hoque, A., Ahsan, M.B.H., 2018. Molecular Docking, Pharmacokinetic, and DFT Calculation of Naproxen and its Degradants. Biomed. J. Sci. Tech. Res. 9, 7360–7364.
Rahman, A., Tuhin Ali, M., Khan Shawan, M.M.A., Golam Sarwar, M., Khan, M.A.K., Halim, M.A., 2016. Halogen-directed drug design for Alzheimer's disease: a combined density functional and molecular docking study. SpringerPlus 5, 1346.
Parr, R.G., Donelly, R.A., Levy, M., Palke, W.E., 1978. J. Chem. Phys. 68, 3801.
Parr, R.G., Szentpaly, L., Liu, S., 1999. J. Am. Chem. Soc. 121, 1922.
Koopmans, T., 1933. Physica 1, 104.
Morris, Garrett M., Huey, Ruth, Lindstrom, William, Sanner, Michel F., Belew, Richard K., Goodsell, David S., Olson, Arthur J., 2009. AutoDock4 and AutoDockTools4: Automated docking with selective receptor flexibility. J. Comput. Chem. 30 (16), 2785–2791.
Aghaei, Mehrdad, Ramezanitaghartapeh, Mohammad, Javan, Masoud, Hoseininezhad-Namin, Mir Saleh, Mirzaei, Hassan, Rad, Ali Shokuhi, Soltani, Alireza, Sedighi, Sima, Lup, Andrew Ng Kay, Khori, Vahid, Mahon, Peter J., Heidari, Fatemeh, 2021b. Fatemeh Heidari, Investigations of adsorption behavior and anti-inflammatory activity of glycine functionalized $Al_{12}N_{12}$ and $Al_{12}ON_{11}$ fullerene-like cages. Spectrochimica Acta Part A 246, 119023. https://doi.org/10.1016/j.saa.2020.119023.
Cao, Yan, Khan, Afrasyab, Mirzaei, Hassan, Reza Khandoozi, Seyed, Javan, Masoud, Ng Kay Lup, Andrew, Norouzi, Alireza, Tazikeh Lemeski, E., Pishnamazi, Maedeh, Soltani, Alireza, Albadarin, Ahmad B., 2021. Investigations of Adsorption Behavior and Anticancer Activity of Curcumin on Pure and Platinum-Functionalized $B_{12}N_{12}$ Nanocages. J. Mol. Liq. 334, 116516. https://doi.org/10.1016/j.molliq.2021.116516.
Cao, Yan, Khan, Afrasyab, Soltani, Alireza, Erfani-Moghadam, Vahid, Lup, Andrew Ng Kay, Aghaei, Mehrdad, Abdolahi, Nafiseh, Khalili, Mohsen, Cordani, Marco, Balakheyli, Hanzaleh, Tavassoli, Samaneh, Albadarin, Ahmad B., 2021. Spectroscopic, density functional theory, cytotoxicity and antioxidant activities of sulfasalazine and naproxen drugs combination. Arabian J. Chem. 14 (6), 103190. https://doi.org/10.1016/j.arabjc.2021.103190.
Cao, Y., Khan, A., Balakheyli, H., 2021. A. Ng Kay Lup, M. Ramezani Taghartapeh, H. Mirzaei, S. Reza Khandoozi, A. Soltani, M. Aghaei, F. Heidari, S.M. Sarkar, A.B. Albadarin, Penicillamine functionalized B12N12 and B12CaN12 nanocages act as potential inhibitors of proinflammatory cytokines: A combined DFT analysis, ADMET and molecular docking study. Arabian J. Chem. 14, 103200.
Rezvantalab, S., Moraveji, M., Khedri, M., Maleki, R., 2020. An Insight into The Role of Riboflavin Ligand on the Self-assembly of Poly (lactic-co-glycolic acid)-based Nanoparticles, A Molecular Simulation and Experimental Approach. Soft Matter 16, 5250–5260.
Shah Md. Abdur Rauf, Per I. Arvidsson, Fernando Albericio, Thavendran Govender, Glenn E. M. Maguire, Hendrik G. Kruger, Bahareh Honarparvar, The effect of N-methylation of amino acids (Ac-X-OMe) on solubility and conformation: A DFT study, Org. Biomol. Chem. 13 (2015) 9993-10006.
Pasban, S., Raissi, H., 2021. Nanotechnology-based approaches for targeting and delivery of drugs via Hexakis (m-PE) macrocycles. Sci. Rep. 11, 8256.
Mirzaei, H., Shokrzadeh, M., Emami, S., 2017. Synthesis, cytotoxic activity and docking study of two indole-chalcone derivatives. J. Mazandaran Univ. Med. Sci. 27 (154), 12–25.
Mirzaei, H., Keighobadi, M., Emami, S., 2017. An overview of anticancer chalcones with apoptosis inducing activity. J. Mazandaran Univ. Med. Sci. 26 (146), 254–268.

Ermondi, Giuseppe, Caron, Giulia, Lawrence, Raelene, Longo, Dario, 2004. Docking studies on NSAID/COX-2 isozyme complexes using Contact Statistics analysis. J. Comput. Aided Mol. Des. 18 (11), 683–696.

Xu, S., Peng, H., Wang, N., Zhao, M., 2018. Inhibition of TNF-α and IL-1 by compounds from selected plants for rheumatoid arthritis therapy: In vivo and in silico studies. Trop. J. Pharm. Res. 17 (2), 277–285.

Daze, K., & Hof, F. (2016). Molecular interaction and recognition. Encyclopedia of physical organic chemistry, 5 Volume set (1st ed.). John Wiley & Sons, Inc.

V. Srivastava, A. Yadav, P. Sarkara, Molecular docking and ADMET study of bioactive compounds of Glycyrrhiza glabra against main protease of SARS-CoV2, Mater Today Proc. (2020).